

# OPTICAL EMISSION SPECTROSCOPY OF PLASMA FORMATION IN A XENON THETA PINCH

W. Meeks <sup>ξ</sup>, R. Pahl, and J. Rovey

Missouri University of Science and Technology, 400 W. 13<sup>th</sup> St.  
Rolla, Missouri, 65409, USA

## Abstract

Analyses of xenon spectral emission data in the IR range primarily from Xe I transitions and estimations of electron temperature are performed on a theta pinch test article. Estimations are based on a collisional-radiative model originally written for Hall-effect thrusters by Karabadzhak et al. which takes into account metastable species in the 1s excited state of xenon. Tests performed on a pulsed xenon plasma at an energy of 80 joules, neutral back-fill pressures of  $10^{-2}$  to  $10^{-1}$  Torr, and discharge frequency of 460 kHz yield electron temperatures of 6.5 to 11.3 eV for cumulative spectra in the first 20  $\mu$ s. Spectra acquired in the UV range verify the presence of 2<sup>nd</sup> order diffraction from Xe II transitions. Low single-to-noise ratios for optical gate widths of 250 nanoseconds produce substantial fluctuation in intensities and thus estimation errors, while not quantified here, are assumed high.

## I. INTRODUCTION

Pulsed inductive plasma (PIP) devices such as the theta-pinch coil are a type of high energy plasma source used in both research and industry. In recent years, PIP devices currently being investigated by the fusion and space propulsion communities utilizing deuterium and xenon, respectively, have provided promising new results.[1], [2] Despite these and many other efforts to utilize PIP devices, a substantial knowledge gap remains with respect to the energy conversion processes during the early plasma formation times. All of the energy in a PIP discharge originates as stored electrical energy. However, by the end of the devices operational cycle that energy has been divided among radiative losses (light emission, x-rays, stray capacitance/inductance), joule heating (of both the device and the gas), unusable directions in bulk fluid motion (via poor containment or undesired expansion upon expulsion), and collisional processes. These can be divided further still into numerous electronic modes, many of which do not provide a direct path to ionization. The net effect of these losses is increased ionization costs and reduced effectiveness of the device.

The broad efforts of this research are to elucidate the electric-to-particle energy conversion processes during the initial plasma formation over time scales of  $10^{-8}$  to  $10^{-6}$  seconds. These time-scales represent 1/100th to 1 discharge oscillation cycle of the Missouri Plasmoid Experiment (MPX), which has a characteristic frequency of approximately 500 kHz in vacuum.

## II. TEST ARTICLE

First the inductive test article is described, followed by the spectral data acquisition equipment and its arrangement.

### A. Theta-pinch Device

A photo of the MPX device with call-outs can be seen in Fig. 1. MPX is a theta-pinch configuration PIP test article with evacuated cylindrical dimensions of 91.5 cm length by 15.5 cm inner diameter for a volume of 1,418  $\text{cm}^3$  and a length-to-diameter (L/D) ratio of 5.90.[3], [4] The theta-pinch coil itself, constructed from a rolled sheet of 1.5 mm thick copper, spans approximately 83% of the evacuated length at 76.2 cm and has an inner diameter of 17.8 cm. The discharge circuit consists of a single Maxwell Technologies 0.7  $\mu\text{F}$ , 40 kV rated high-energy capacitor and a Perkin-Elmer GP-14B spark-gap trigger. A DC glow discharge electron source was placed at one end of the discharge chamber out of the line-of-sight of the optical emission pick-up to assist in plasma formation and reliability. The DC source was maintained at approximately 50 volts. Figure 2 shows two typical

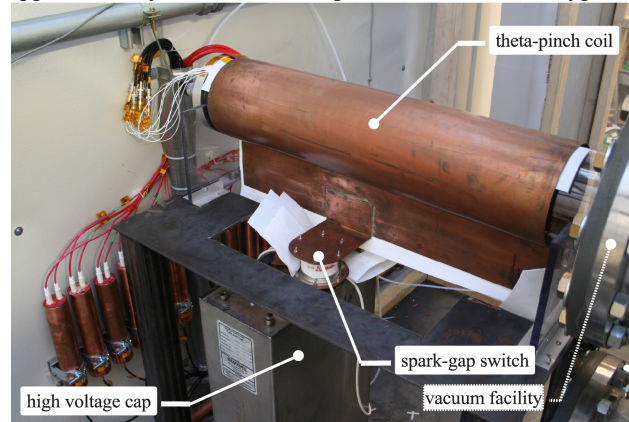
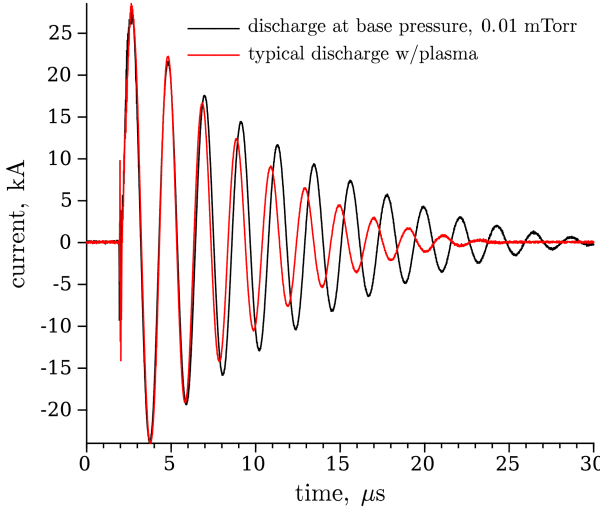


Figure 1. Missouri Plasmoid Experiment, (optical fiber not shown).

<sup>ξ</sup> email: wcm994@mst.edu

current discharge profiles, a vacuum (i.e., no plasma) case and the other when plasma is present. Attenuation due to mutual inductance can be observed when plasma is present, and this is a well-known effect observed in similar devices.[5] This mutual inductance affects the discharge profile two-fold; 1.) it reduces the LRC time-constant and 2.) it increases the discharge frequency.



**Figure 2.** Typical MPX discharge profiles with and without plasma. Time zero represents when the DAQ received its trigger subsequently showing a delay of around 2  $\mu$ s before capacitor discharge occurred.

### B. Optical Emission Acquisition

The optical emission spectroscopy (OES) equipment used here consisted of: (1) a Princeton Instruments SP-2356 Czerny-Turner spectrometer with a 0.3 meter focal length, triple grating turret with gratings of 300, 1200, and 2400 g/mm, and a 14 mm high slit with width adjustable from 10  $\mu$ m to 3 mm. Grating and slit width used here were 300 g/mm and 50  $\mu$ m, respectively. (2) a PI-MAX intensified CCD camera with 1024 by 1024 pixel array. (3) a ST-133 controller with built-in PTG trigger module for repetitive (used in this work) or sequential external triggering. Light emission was transmitted from the experiment to the spectrometer slit via a 7.5 meter long, 200 micron core, VIS/NIR (low OH) Ocean Optics fiber. The fiber was mounted perpendicular to the coil axial direction pointing toward the center of the discharge tube. Fig. 3 provides further clarification of this orientation. A 3 to 5 shot 'cleansing' procedure was needed to remove contaminant spectra from the data after any repressurization to atmosphere. This has been encountered before in PIP device operation and is generally thought to be the result of oxygen deposition to the inner quartz chamber walls. This cleansing procedure was used for all pressures.

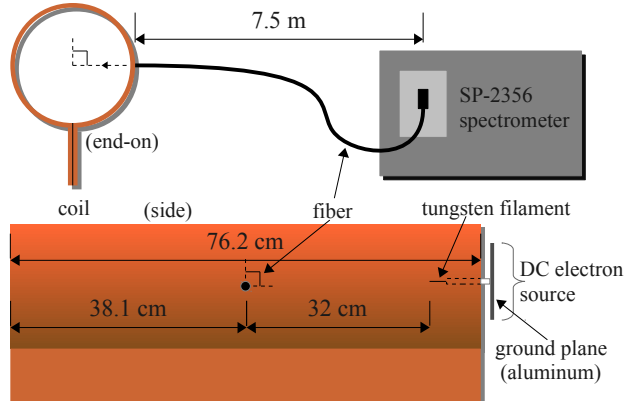


Figure 3: Optical fiber and DC source orientation.

## III. EXPERIMENTAL RESULTS

### A. Raw Spectral Data

Pressures of 10, 30, 50, and 100 mTorr were tested using xenon back-filled from approximately 0.1 mTorr. Two different spectral data sets were acquired at each of these pressures for xenon. The first set were long-exposures of 20  $\mu$ s to capture all dominant plasma activity over the entire discharge. Four to five of these spectra were acquired per pressure and then averaged. Figure 4 shows the results of these averaged long-exposures for each pressure. Vertical (intensity) scales for all graphs in Fig. 4 though not shown are equal. The second set of data were obtained to provide a time-resolved intensity profile. These were captured at fixed CCD gate widths of 250 ns each and gate delays starting from approximately the initial trigger,  $t_0$  (actually  $t = t_0 + 30$  ns due to machine delay) to the full 20  $\mu$ s. Thus time-marching a viewing window of 250 ns forward to build the time-resolved profile. At each delay between two and five spectra were acquired depending on whether or not plasma activity was observed. Multiple spectra per delay were acquired to allow for an average to be taken for a given delay. This averaging was deemed necessary due to a significant temporal jitter found from discharge to discharge of up to 100 ns. This contributes to high errors expected in electron temperature calculations from ratios for the short duration spectra while expected to contribute little to long duration spectra. While it was common in previous studies to see no significant plasma activity until approximately the first 'zero-crossing' of the current,[6] the addition of a DC glow discharge has enabled earlier formation and observation of plasma as current initially increases at  $t = t_0 + 2$   $\mu$ s.

Six of the eight IR transition lines reported in Chiu et al.[7] were measured in this experiment. Namely the 823.2, 828.0, 834.7, 881.9, 904.5, and 916.3 nm transition lines. The 823.2 nm line (referred hereto as the 823 line) representing the  $2p_6$  to  $1s_5$  transition (in Paschen notation) proved to be the most reliable due to high signal-to-noise ratio (SNR) and so for brevity is the

transition of focus for the work presented here. Figure 5 shows raw intensity data, averaged for the number of shots at each gate delay, then time-resolved for the 823 line at each pressure. In addition to the raw data a spline fit is superimposed to provide an overall trend for each pressure. These spline fits were used to create the ratio profiles for numerical analysis.

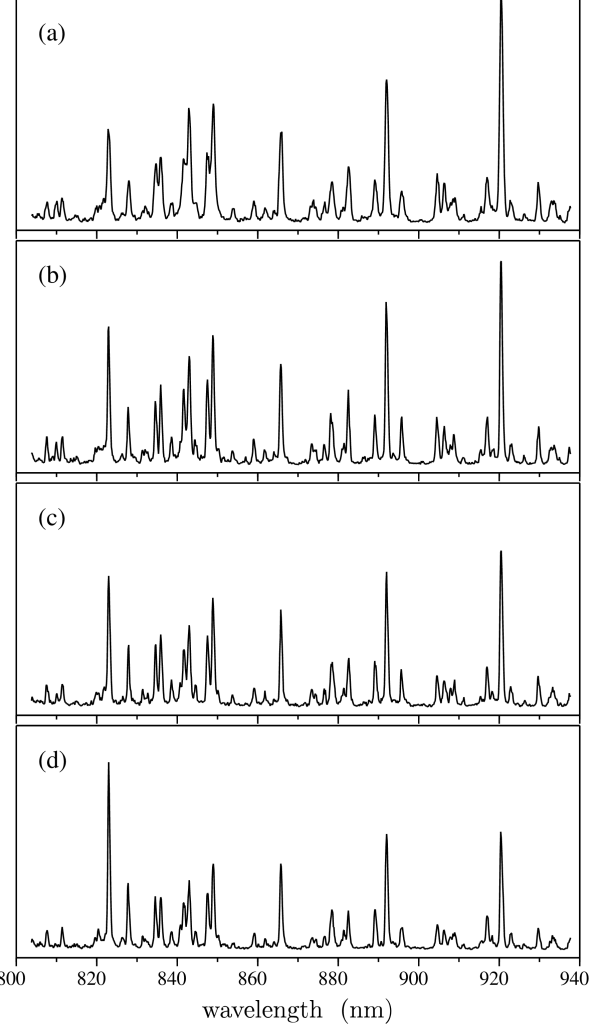


**Figure 4.** 20  $\mu$ s MPX discharge exposures for xenon at; (a) 10 mTorr, (b) 30 mTorr, (c) 50 mTorr, and (d) 100 mTorr.

### B. Post-Processing

Inspection of the 20  $\mu$ s spectral data shown in Fig. 4 shows that Xe I alone can not account for all dominant lines observed. Since a grated spectrometer was used, and no 2<sup>nd</sup> order filters were in place, looking in the UV bandwidth proved necessary to provide confirmation of 2<sup>nd</sup> order diffraction from ionized Xe species transitions. Figure 6 shows the results of long-exposure discharges in the wavelength range of 357 to 496 nm for 50 mTorr

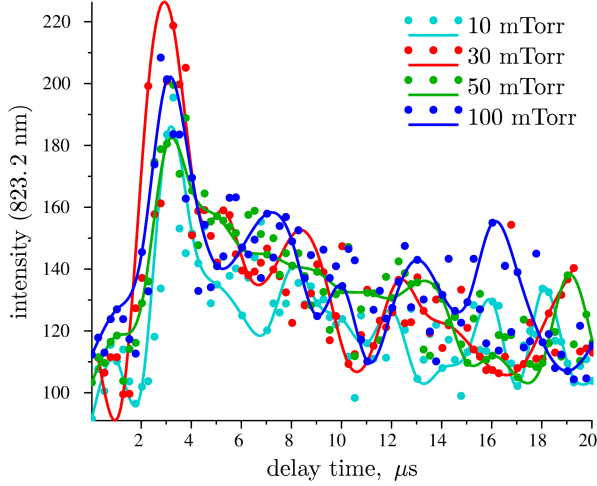


**Figure 5.** Averaged, time-resolved data for the 823.2 nm at each of the four pressures tested in this work.

xenon as well as 50 mTorr in air. Pressures of 10, 30, and 100 mTorr were identical with regard to dominant lines. Figure 6a shows xenon data for three tests while Fig. 6b shows air data for three tests. Analysis of Fig. 6 shows two important results; 1.) all dominant lines unaccountable in the IR band by Xe I can be accounted for in first order in the xenon UV band (400 to 470 nm), and 2.) comparison between the two sub-figures shows no lines in common suggesting that contamination during xenon testing by air constituents does not occur.

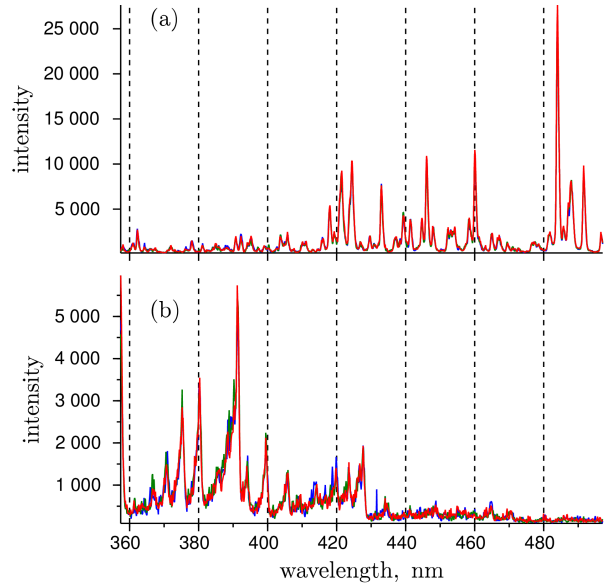


**Figure 6.** UV spectra (3 sets each) for MPX at 50 mTorr in; (a) xenon, and (b) air.

All dominant lines in the IR range (approximately 803 to 938 nm) can be accounted for by taking into account 2<sup>nd</sup> order diffraction from ionized Xe species transitions. Observed xenon UV spectra are cross-referenced with the National Institute of Standards and Technology (NIST) spectral database from which the dominant lines are attributed to transitions from singly ionized xenon species, Xe II. Figure 7 shows this accountability for 50 mTorr and once again the 10, 30, and 100 mTorr cases can be handled identically. Blue and red data points shown in Fig. 7 represent tabulated lines from the NIST database, for Xe I and Xe II, respectively. Second order Xe II lines and dominant Xe I lines are within less than 0.1% of NIST data except for an 935.3 nm line. This single exception is being attributed to the curve fit used in wavelength calibration of the CCD array.

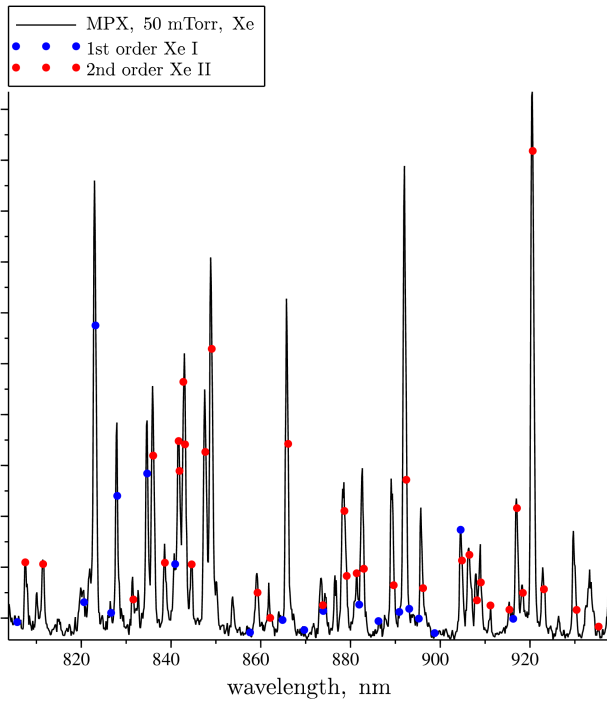


**Figure 7.** Long-exposure discharge of MPX at 50 mTorr xenon. Dominant peaks are all accounted for by taken into account 2nd order diffraction of Xe II.

## IV. NUMERICAL ANALYSIS

### A. Collisional-radiative Model

Electron temperatures are approximated via intensity ratios estimated by the Karabazhak et al.[8] collisional-radiative model (KCD model). The KCD model utilizes experimentally obtained cross-section data [7], [9], [10] in the collisional probability calculation of neutral excited species via electrons, singly ionized, and doubly ionized xenon atoms. Endorsed by the authors of the original KCD model, xenon cross-sections for direct neutral

excitation from Fons and Lin,[10] were used here to extend the applicability of the model from collisional energies of 70 eV to 150 eV. The data of Fons and Lin undergo both a zero-pressure correction and an optical opacity correction as outlined in Karabazhak et al.,[8]. Electrons are assumed Maxwellian. Line intensity per unit volume for a given wavelength is approximated by,

$$J_\lambda(\text{Xe I}) = \frac{hc}{4\pi\lambda} N_0 N_e \left( k_e^\lambda + \alpha \cdot k_1^\lambda + \frac{1-\alpha}{2} k_2^\lambda \right) B^\lambda \quad (1)$$

where  $N_0$  and  $N_e$  are the number densities of all xenon atoms and electrons, respectively.  $k_1$  and  $k_2$  are the emission excitation rate coefficients for impact between neutrals and  $\text{Xe}^+$ ,  $\text{Xe}^{2+}$ , respectively, and  $\alpha = N_1/N_e$ . The parameter,  $B^\lambda$ , in Eq. 1 represents a correction factor as defined in Karabazhak et al.[8] and is dependent on the  $1s_5$  metastable population.

### B. Temperature Approximations

Analysis of each of the averaged 20  $\mu\text{s}$  spectra shown in Fig. 4 is provided in Table 1, linearly interpolated from model data. From Table 1 the average electron temperature over the full discharge can be seen to range from 6.5 to 11.3 eV.

**Table 1.** Electron temperature approximations for MPX at discharge voltage and frequency of 15 kV and 460 kHz, respectively, based on the xenon 823.2 to 828.0 nm ratio in the 20  $\mu\text{s}$  (long-exposure) spectra of Fig. 4.

Pressure (mTorr)	$(823/828)_{20\mu\text{s}}$	$T_{e,\text{KCD}}$ (eV)
10	2.8	6.5
30	2.2	10.0
50	2.1	11.3
100	2.6	7.2

Figure 8a shows time-resolved temperatures approximated with the KCD model using the 823 to 828 line ratio and assuming a 2.0% tolerance against the models predicted ratios. Data are calculated at every 250 ns starting from 2.03  $\mu\text{s}$  up to 6.03  $\mu\text{s}$ . Data points are temperatures calculated from the data directly while trend lines are calculated using ratios of the cubic spline fits mentioned in Sec. IIIB and shown in Fig. 5. Areas where no data appear for a given pressure and time are out of the range predicted by the model (i.e., the ratio calculated would put it above 150 eV based solely on the model trend at high temperatures). Figure 8b shows a coil discharge profile in the same time frame for reference. Electron temperature estimates in the time frame shown range nearly the entire scope of the model from 135.5 eV in 10 mTorr at 2.5  $\mu\text{s}$  down to 7.5 eV in 50 mTorr at 4.5  $\mu\text{s}$ .

### C. Discussion

Table 1 provides the most accurate electron temperature data on average. The line ratio method can be very susceptible to error in a low SNR environment and inspection of Fig. 4 yields SNR values of 9.5 and 5 for the 823.2 and 828 lines, respectively, for the long-exposure spectra. In contrast the short exposures of 250 ns had typical SNR values ranging from less than 2.5 up to 5. From Fig. 8 a couple of observations may be made. First is the presence of high electron temperature peaks (of greater than 100 eV at some points). These peaks from the high fluctuation in estimated electron temperature are within the realm of those reported for PIP devices,[11], [12]. However, the basis of these predictions must also be considered. These predictions are based on a ratio of intensities calculated from a relatively short time frame of 250 nanoseconds where the SNR can be quite low. With  $\text{SNR} < 2.5$  ( $< 4 \text{ dB}$ ) at times of low plasma activity and  $\text{SNR} \approx 5.0$  ( $\approx 7 \text{ dB}$ ) during high activity.

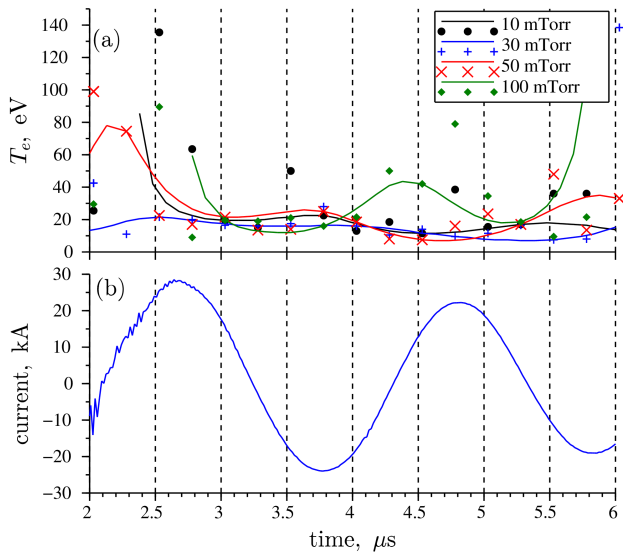


**Figure 8.** (a) MPX electron temperature estimates based on the Karabadzhak et al. model and ratio analysis of 823.2 nm to 828 nm lines from 2 to 6  $\mu\text{s}$ . (b) typical coil current discharge profile during the same time frame.

Secondly, the peak temperatures appear to coincide with local minima and maxima in discharge current. This correlates well with the above observation and the findings of the author's previous work which has shown that plasma activity in a PIP device is hindered in the presence of large magnetic fields due to restrictions in charge carrier mobility.[6] From Faraday's law, magnetic field is directly proportional to current in an inductive coil geometry. Put another way; times when electron temperatures appear to peak correspond approximately to when the errors due to low SNR would be highest.

In addition to this, electron temperature estimates for both the long and short duration spectra are expected to have high levels of error due to the averaging performed for each set of spectra. Because the cumulative plasma activity is not observed to change from discharge to discharge, this averaging error will have less affect on the long 20  $\mu\text{s}$  acquisitions than on the short 250 ns acquisitions.

## V. CONCLUSIONS

IR and UV spectra were acquired for a pulsed theta-pinch xenon plasma at 10, 30, 50, and 100 mTorr. The IR band, specifically the most intense transition lines of 823.2 and 828.0 nm from the  $2p$  to  $1s$  sub-shells, were utilized for a line ratio technique to estimate electron temperature. Lines unaccountable by 1<sup>st</sup> order Xe I transitions in the IR band were accountable by 2<sup>nd</sup> order Xe II transitions observed in the UV band. The collisional-radiative model developed by Karabadzhak et al. to describe Hall-effect thrusters was used to estimate electron temperatures from the a fore mentioned line ratio. Cumulative total discharge spectra yield temperatures ranging from 6.5 to 11.3 eV. High noise fast spectra (CCD gate width = 250 ns) yield temperatures ranging from 8 to 136 eV with peak temperatures coinciding approximately with coil current peaks.

## VI. ACKNOWLEDGMENTS

We would like to thank Dr. Scott Kovaleski at our sister campus; University of Missouri – Columbia, for the use of his OES equipment that made this work possible, AFOSR for their continued funding (award# FA9550-10-1-0204), and Dr.'s Dan Brown, Carrie Hill, and Ben Prince for their continued input and suggestions.

## VII. REFERENCES

- [1] G. Wurden, "FRCHX Magnetized Target Fusion HEDLP Experiments," presented at the 22nd Fusion Energy Conference, Geneva, Switzerland, 2008.
- [2] D. Kirtley, J. Slough, M. Pfaff, and C. Pihl, "Steady Operation of an Electromagnetic Plasmoid Thruster," in *8th MSS/5th LPS/5th SPS Joint Subcommittee Meeting*, 2011.
- [3] R. Pahl and J. Rovey, "Pre-Ionization Plasma in a FRC Test Article," presented at the 50th Aerospace Sciences Meeting, Nashville, TN, 2012.
- [4] R. Pahl, W. Meeks, and J. Rovey, "Magnetic Field Mapping of a Field Reversed Configuration Test Article," presented at the 47th Joing Propulsion Conference, San Diego, CA, 2011.

- [5] K. Polzin, M. Rose, and R. Miller, “Operational Characteristics of a Low-Energy FARAD Thruster,” 2008.
- [6] W. C. Meeks and J. L. Rovey, “On the delayed gas breakdown in a ringing theta-pinch with bias magnetic field,” *Phys. Plasmas*, vol. 19, no. 5, pp. 052505–052505–7, May 2012.
- [7] Y. Chiu, B. L. Austin, S. Williams, R. A. Dressler, and G. F. Karabadzhak, “Passive optical diagnostic of Xe-propelled Hall thrusters. I. Emission cross sections,” *J. Appl. Phys.*, vol. 99, no. 11, pp. 113304–113304–11, Jun. 2006.
- [8] G. F. Karabadzhak, Y. Chiu, and R. A. Dressler, “Passive optical diagnostic of Xe propelled Hall thrusters. II. Collisional-radiative model,” *J. Appl. Phys.*, vol. 99, no. 11, pp. 113305–113305–12, Jun. 2006.
- [9] J. Sommerville, “Emission Cross Sections for Neutral Xenon Impacted by Xe<sup>+</sup> and Xe<sup>2+</sup>,” Michigan Technological University, 2006.
- [10] J. T. Fons and C. C. Lin, “Measurement of the cross sections for electron-impact excitation into the 5p<sup>5</sup>{5}6p levels of xenon,” *Phys. Rev.*, vol. 58, no. 6, pp. 4603–4615, Dec. 1998.
- [11] S. Zhang, G. A. Wurden, T. P. Intrator, E. L. Ruden, W. J. Waganaar, C. T. Grabowski, R. M. Renneke, and J. H. Degnan, “High-density field-reversed configuration plasma for magnetized target fusion,” *Ieee Trans. Plasma Sci.*, vol. 34, no. 2, pp. 223–228, 2006.
- [12] B. Kronast, H. Röhr, E. Glock, H. Zwicker, and E. Fünfer, “Measurements of the Ion and Electron Temperature in a Theta-Pinch Plasma by Forward Scattering,” *Phys. Rev. Lett.*, vol. 16, no. 24, pp. 1082–1085, Jun. 1966.